journal

J. Am. Ceram. Soc., **82** [2] 366–72 (1999)

Investigating the Structure–Property Relationships at Grain Boundaries in MgO Using Bond–Valence Pair Potentials and Multiple Scattering Analysis

Nigel D. Browning,*,† James P. Buban,† Habib O. Moltaji,† and Gerd Duscher†,‡

Department of Physics, University of Illinois at Chicago, Chicago, Illinois 60607-7059; and
Solid State Division, Oak Ridge National Laboratory, Oak Ridge, Tennessee 37831-6030

We describe the use of bond–valence analysis to investigate the segregation of calcium atoms at an MgO [001] tilt grain boundary. For small deviations away from the equilibrium metal-oxide bond length, the bond–valence parameter approximates well to a Born–Mayer-type pair potential. Therefore, by starting with a structural model determined from an atomic resolution Z-contrast image, compositional and cation valence state information obtained from electron energy loss spectroscopy (EELS) can be incorporated into a comprehensive model for the grain boundary. For the boundary under investigation here, it is found that specific sites for preferential segregation can be identified, resulting in 0.3–0.4 monolayers of calcium in the boundary plane.

I. Introduction

OXIDE materials are currently being developed for such diverse electronic applications as varistors,[1] ferroelectrics,[2] and high-T_c superconductors.[3] Although varied systems are being utilized for each application, they are all linked, either by accident or design, to a fundamental issue: the formation of atomic-scale defects, such as lattice vacancies, dislocations, stacking faults, and grain boundaries, during fabrication. The effects of most of these defects can be modeled by considering their equilibrium distribution within the bulk.[4] Grain boundaries, however, inherently contain a concentration of defects far in excess of equilibrium distribution in the bulk of the material.[5] This excess of defects results in the boundary having a different atomic arrangement to the bulk and, in many cases, radically different properties. Hence, although grain boundaries account for only a small fraction of the material, they can have far-reaching consequences for the overall bulk-scale electrical and mechanical properties. To fully develop the desired technological application of a particular material, it is therefore necessary to achieve a fundamental understanding of the properties of grain boundaries.

The usual methods of investigating the structure–property relationships of grain boundaries are either phase contrast imaging[6–9] in the transmission electron microscope (TEM) or Z-contrast imaging[10–12] in the scanning transmission electron microscope (STEM). While both of these techniques allow a structural model to be determined, they do not necessarily allow us to formulate the properties of the boundary, as compositional and electronic structure fluctuations can also be important. Using analytical techniques, such as energy dispersive X-ray spectroscopy (EDS)[13] and electron energy loss spectroscopy (EELS),[14] these fluctuations can be quantified and a more complete analysis of the boundary obtained. Furthermore, the recent development of electron holography techniques[15] permits any electrical barrier formed at the grain boundary to be directly imaged. There is, therefore, a wealth of experimental information that can be acquired from any individual grain boundary. However, to understand the structure–property relationships on the fundamental atomic scale, we must combine all of this information into a single model for the boundary. While this is usually accomplished by the use of theoretical calculations, many of the computational methods are limited to the study of boundaries with short repeat length.[16,17] This type of boundary is usually not prevalent in materials used for technological applications, leading to a gap between what can be reasonably computed and what really exists in materials. To bridge this gap, we need to develop a more general theoretical method that allows us to deal with all boundary structures.

In this paper we describe the use of bond–valence sum analysis to develop atomic-scale models of grain boundaries, on which the understanding of the structure–property relationships can be based. The bond–valence methodology is derived from Pauling's rules.[18] These basic concepts have been developed further by Brown[19] to produce an equation for the bond strength between two atoms in the form

$$S = \exp\left(\frac{r_{ij} - r_0}{B}\right) \tag{1}$$

where r_0 is a reference bond length for a given pair of atoms (in a given oxidation state) and B a constant (0.37) determined by fitting to a wide range of crystal data.[20,21] The formal valence state of an atom is then simply the sum of the contributions from each bond ($V = \Sigma S$). A further refinement of this analysis states that all of the bonds should be as equal as possible.[19] The form of this function is essentially the same as a Born–Mayer-type potential for small distortions away from the equilibrium bond length.[22] Using bond–valence as a simple pair potential, we are, therefore, in a position to incorporate the experimental quantification of the structure, composition, and valence state at grain boundaries into a single model.

The use of this analysis is demonstrated here for a 27° [001] tilt grain boundary in MgO. In this case, although the Z-contrast image[23] shows that the boundary is atomically abrupt, the presence of segregated calcium impurities in the boundary plane is detected by EELS. Using the bond–valence technique, the most likely atomic sites in the boundary plane for calcium segregation are located. Additionally, the analysis predicts that 0.3–0.4 monolayers of calcium at the boundary are necessary to stabilize the structure in the form observed in the image, consistent with experimental EELS results. Furthermore, analysis of the fine structure of the energy loss spectrum from the region of the calcium segregants indicates that the electronic structure

R. H. French—contributing editor

Manuscript No. 190363. Received February 20, 1998; approved May 26, 1998.
Supported by U.S. Department of Energy under Grant No. DE-FG02-96ER45610.
*Member, American Ceramic Society.
†University of Illinois.
‡Oak Ridge National Laboratory.

is consistent with the formation of CaO at these locations. Such analysis suggests that even on the atomic scale, the properties of the grain boundary can be interpreted in terms of the presence of CaO precipitates in the boundary plane.

II. Experimental Results

The use of the Z-constrast imaging technique to determine the structure of the 27° [001] tilt grain-boundary plane in a bicrystal sample has been discussed previously in detail by Yan *et al.*[23] Figure 1 shows the schematic structure of the boundary that was developed from the image. Energy loss spectra obtained from the region of the grain boundary are shown in Fig. 2. These spectra are acquired using the spatial difference technique[24] and show the presence of calcium segregants at the grain boundary. By comparing the intensity of the calcium *L*-edge with the oxygen *K*-edge using the areal density method,[25] the concentration of calcium in the boundary is determined to be ~0.3–0.4 monolayers. The oxygen *K*-edge spectrum obtained from the region of the boundary shows no significant changes from the bulk. This experimental result implies there should be only minor changes in the oxygen coordination at the boundary (see Discussion). As calcium has only one formal valence state, we can assume that the segregants at the boundary do not cause any local charge imbalance (magnesium and calcium have a 2+ valence state). No trace of other impurities at the boundary are found using EELS or EDS.

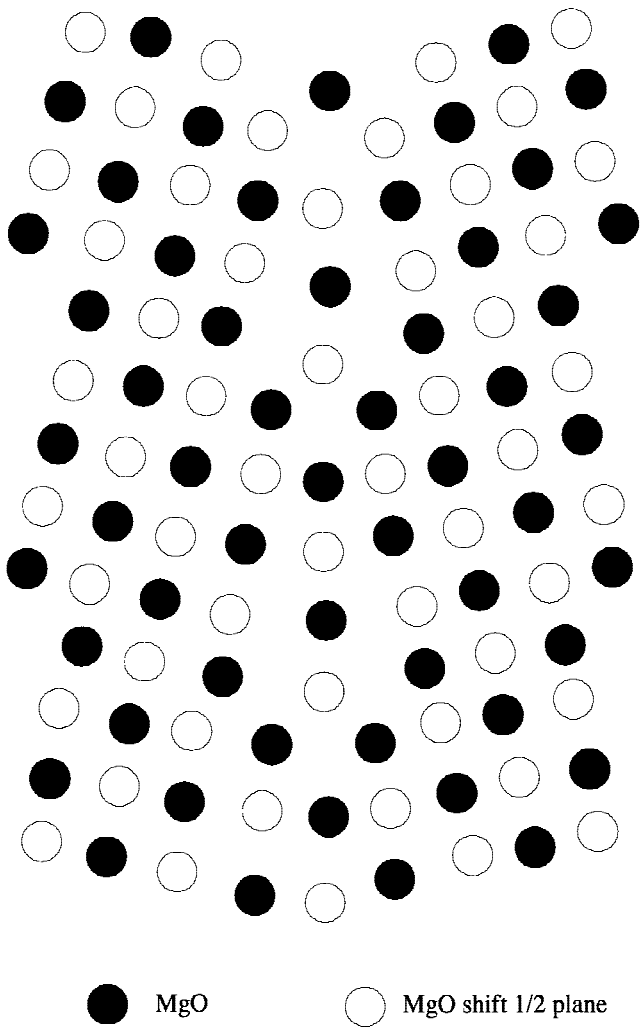

Fig. 1. Schematic of the 27° [001] tilt grain boundary in MgO. In this orientation of the rocksalt structure, the columns of atoms contain magnesium and oxygen with a nearest neighbor distance of 2.1 Å.

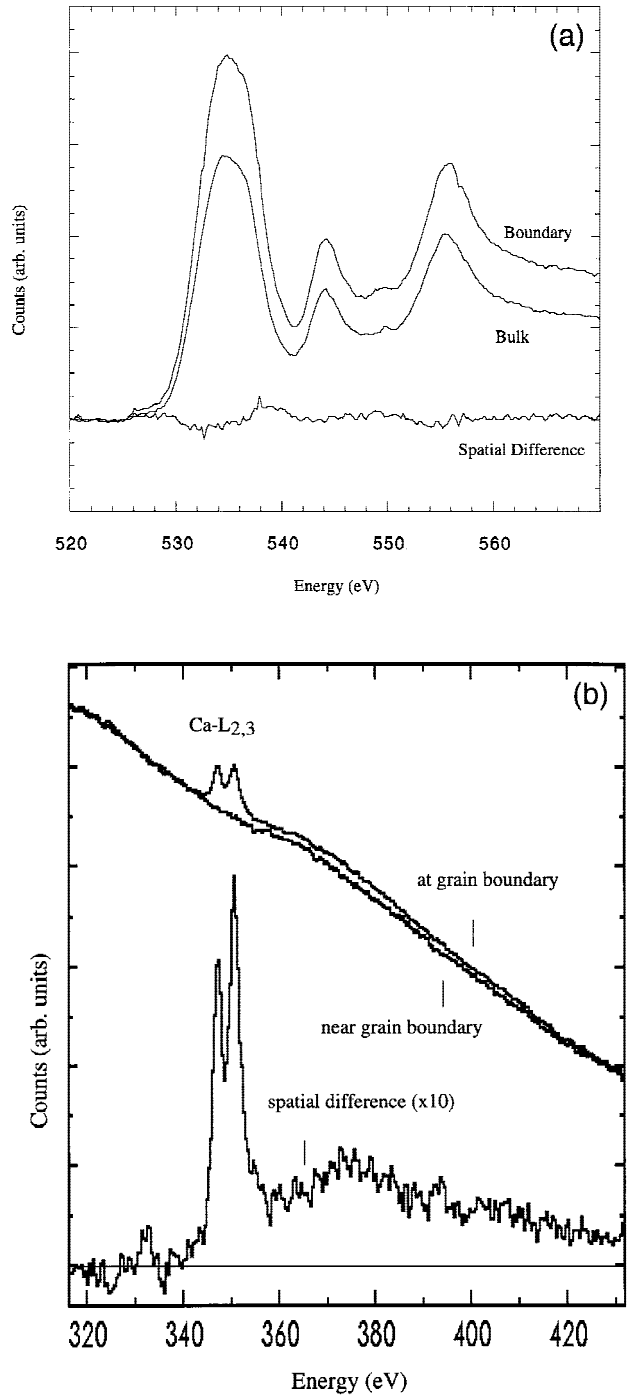

Fig. 2. (a) Oxygen *K*-edge and (b) calcium *L*-edge spectra from the bulk and boundary.

III. Bond–Valence Analysis Method

The aim of this paper is to demonstrate a means of incorporating the structure, composition, and cation valence state determined experimentally into a single model for the grain boundary. While there are many ways of doing this, pair potentials are commonly used to investigate the structure–property relationships of materials[26,27] in order to avoid the high-symmetry requirements and computational time of band–structure calculations.[16,17] One of the more frequently used pair potentials is the Born–Mayer type[23] (which is particularly appropriate here considering the ionic nature of MgO), which is given by

$$\Phi(r_{ij}) = \frac{q_i q_j}{r_{ij}} + B_{ij} \exp\left(\frac{-r_{ij}}{\rho_{ij}}\right) + \frac{C_{ij}}{r_{ij}^{\,6}} \tag{2}$$

where B_{ij}, C_{ij}, and ρ_{ij} are adjustable parameters[28] determined by fitting to an experimentally observed structure, q_i and q_j the charges on each of the ions, and r_{ij} the separation of the ions. The first term in the potential is the electrostatic interaction, which is repulsive for like ions and attractive for unlike ions. The second term is the repulsive interaction caused by the Pauli exclusion principle, and the third term is the van der Waals attraction between two atoms.

In this paper, we chose to use the more simple bond–valence parameter defined by Brown.[19] In using this as a potential, it has the following form for a given interaction between two ions

$$\Phi(r_{ij}) = \exp\left[\left(\frac{r_{ij} - r_0}{B}\right) \pm \frac{V}{N}\right]^2 \pm \frac{V}{N} \tag{3}$$

where V is the formal valence, N the coordination number, B a constant (0.37)[20,21] determined by fitting to a large crystal data set, r_0 an equilibrium bond length for a given ion pair, and r_{ij} the separation of the ions. Although this formulation is meant to be used primarily for the interaction between cations and anions, it is possible to define an interaction parameter for like ions by fitting an r_0 value for each structure type. In the same manner as the Born–Mayer potential, we can therefore deal with attractive and repulsive interactions.

Figure 3 shows a comparison between the Born–Mayer potential and the bond–valence potential for MgO. In the region of equilibrium bond length, the two potentials have the same form. Furthermore, the repulsive part of each potential is virtually identical. This should not be surprising, since both the Born–Mayer and bond–valence repulsive interactions are given by an exponential dependence. The main difference between the two potentials is the attractive term, with the bond–valence parameter having a much shallower potential well. What this means for the analysis of grain-boundary structures is that we cannot determine the lowest energy boundary structure without a priori information using the bond–valence parameter. However, this is not a concern in the application here, since we are analyzing structures for which we have an image. In the Z-contrast technique, it is possible to directly determine the atomic positions to within 0.2 Å.[12] This is well within the limit where the bond–valence potential is in good agreement with the Born–Mayer potential. It should also be pointed out that, although this potential deals with ions and implies ionic bonding is a necessity, this is not entirely the case. Every element can be assigned a formal valence state, whether its bonding is ionic or covalent, meaning that the potential can be used in all cases.[29]

In the analysis of a grain-boundary structure, the bond–valence method, therefore, allows us to check the structure observed in the image by performing a simple minimization routine. The error in the positioning of the columns by the Z-contrast technique is 0.2 Å, which is the maximum movement we allow for each column in the structure. As the name implies, the only other parameter necessary for minimization to proceed is the valence of the cation. (This defines the r_0 value.) For the MgO boundary analyzed here, we need only consider the r_0 values for the Mg^{2+}–O^{2-} interaction (1.693 Å) and Ca^{2+}–O^{2-} interaction (1.967 Å).[20,21] Hence, minimization allows a shuffling of the atomic columns in the grain boundary within a very small distance (±0.2 Å) to check if they are all consistent with their formal valence. This simple bond–valence parameter on its own, however, does not ensure that we generate the lowest energy structure in the minimization. It is entirely possible in MgO, for example, to generate three short bonds and three long bonds, where the overall valence of the central atom is in good agreement with the formal valence state. To avoid this effect as much as possible, a bond length criterion is also added to the minimization. This bond length minimization ensures that the contributions to the central atom are made up equally from all the surrounding atoms.

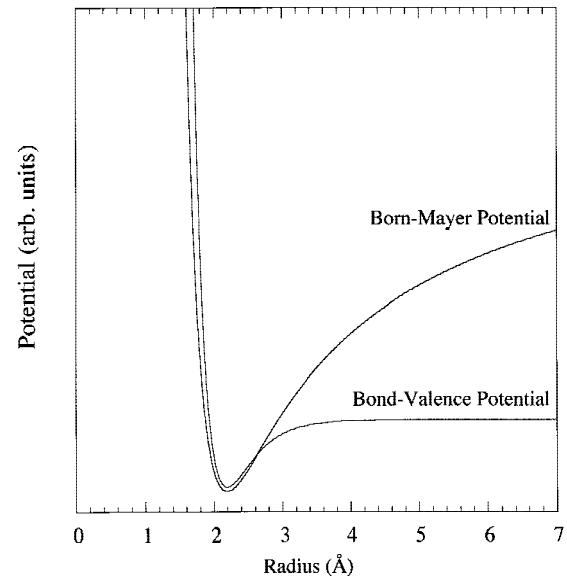

Fig. 3. Comparison of a Born–Mayer-type potential for MgO with the bond–valence parameter. Bond–valence parameter has been scaled to the Born–Mayer potential to show the similarity in the shape of the potential in the region of the equilibrium bond length.

IV. Developing a Structural Model for the Boundary

The starting structure used for the bond–valence sum minimization is shown in Fig. 1. The aim of this minimization is to see if the atomic environments around the atoms in the boundary plane are consistent with their formal valence state. For magnesium and oxygen in the bulk rocksalt structure, the bond–valence calculations give the formal valences as +1.96 and −1.96, respectively. (These values are used for the V/N terms in Eq. (3).) As a first attempt at minimizing the valences of the atoms at the boundaries to these values, we assume that the boundary contains only magnesium and oxygen atoms in the atomic columns. The average values for the valences obtained from this minimization are shown in Table I. Although most of the calculated valences are in reasonable agreement with the bulk values, there are specific locations where they are considerably lower than the bulk values, hence the large standard deviation and low average valence for the result.

The presence of valences that are low in certain positions

Table I. Average Valence for the Boundary Plane as a Function of Calcium Doping

	Number of calcium columns in the boundary plane									
	0		2		3		4		5	
	Mg	O	Mg	O	Mg	O	Mg	O	Mg	O
Average valence	1.69	1.77	1.90	1.92	1.93	1.92	1.90	1.99	1.97	2.05
Standard deviation	0.23	0.28	0.19	0.18	0.09	0.11	0.17	0.37	0.21	0.29

along the boundary indicates that there is a discrepancy between the observed boundary structure and a composition containing only oxygen and magnesium atoms; i.e., we are putting a nominally 2+ or 2− ion into a space large enough for 1+ or 1− ion. This discrepancy can be overcome by substituting a different atom into the boundary site where the valence is low. There are two possibilities that reduce the valence difference: an element of valence 1+ or an element of valence 2+ with a longer equilibrium bond length with oxygen, i.e., a 2+ ion with a larger ionic radius. The EELS results indicate that calcium is present in the boundary and that this is a 2+ ion with a longer equilibrium bond length to oxygen than Mg–O. Placing calcium into the sites that have a lower valence lowers the valence discrepancy. Table I shows the effect of putting increasing numbers of Ca–O columns at the grain boundary. (There are two positions in the structure that have very low valences, and, hence, the first attempt at minimization replaces these two columns with Ca–O.) There is a lowest valence difference condition where 3/8 or 3/9 of the boundary sites contain calcium (Fig. 4). It should be noted that it is impossible to define exactly the fraction of atom sites occupied by calcium from a single image of this boundary, as it is an irrational tilt boundary. The schematic in Fig. 4 shows that there are alternately one and two columns between the dislocation cores. However, the quantified result is in excellent agreement with the quantified EELS measurement from the boundary.[24] Now, however, we have located the calcium atoms at specific sites in the interface and progressed from the basic structural Z-contrast image to a three-dimensional model of the grain boundary that contains compositional changes.

V. Interpreting Electronic Structure

Now that we have a structural and compositional model for the boundary structure, we can start to investigate the effect of these compositional modulations on the local electronic structure. One means to do this is through multiple scattering analysis[30] of the energy loss spectrum. Although multiple scattering theory was originally developed for the analysis of X-ray absorption spectra, its application to EELS is straightforward.[31–34] (Only the method of excitation has changed from an X-ray to an electron). Multiple scattering calculations model the density of unoccupied states (as measured in the experimental spectrum) by considering the scattering of the photoelectron created during the excitation process from neighboring atoms. The many paths that can be taken by a photoelectron alter the matrix elements for a particular transition, because of constructive or destructive interference that occurs between the outgoing and returning photoelectron wave (Fig. 5). In effect, the resultant energy loss spectrum can be described as a simple absorption edge of hydrogenic form, due to an isolated atom, with intensity modulations due to the atomic structure of the solid (Fig. 5); i.e., the absorption $\alpha(E)$ is given by

$$\alpha(E) = \alpha_0(E)\,[1 + \Sigma\, X_n(E)] \qquad (n = 2) \tag{4}$$

where $\alpha_0(E)$ is the atomic absorption and $X_n(E)$ the multiple scattering signal of order n ($n > 1$), which contains all the structural information.[35] Because this description of the unoccupied density of states is based on a real space cluster of atoms, several unique opportunities are presented in this analysis. A lack of symmetry does not seriously affect the calculation, making it ideal for the study of low-symmetry defects, such as grain boundaries. The effects of dopant atoms can be simply investigated by substituting atom types within the cluster and recalculating the scattering. Multiple scattering, therefore, allows spectral changes to be directly interpreted in terms of structural changes. Using this methodology, we can, therefore, check the structural model for the boundary developed from the image and bond–valence analysis and use this structure to draw conclusions on the electronic properties of the boundary.

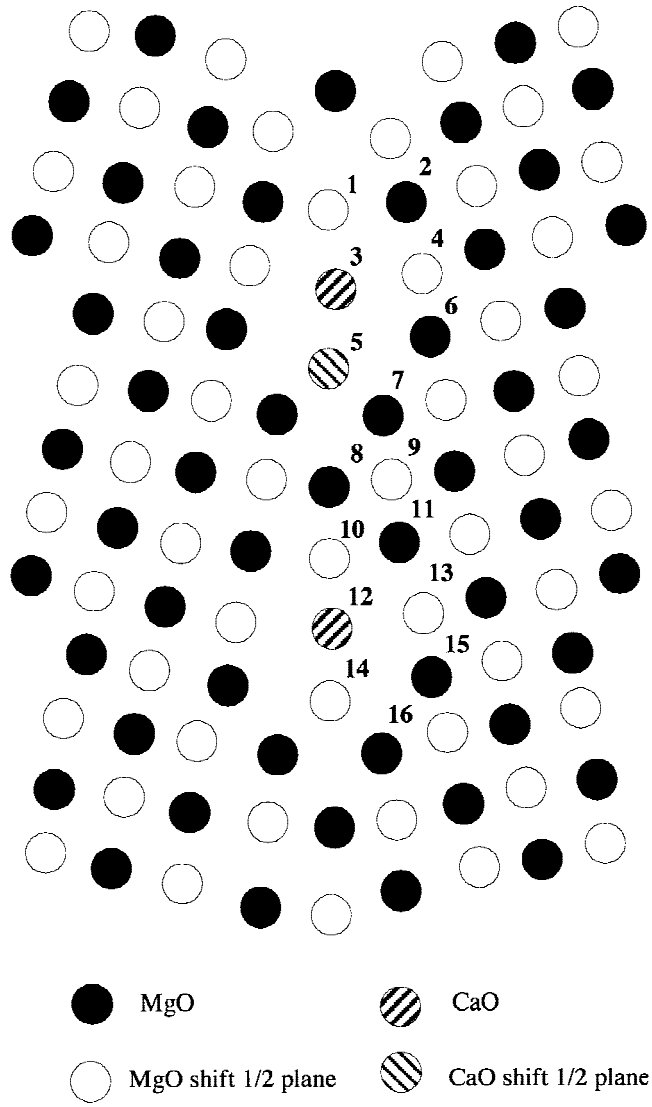

Fig. 4. Schematic of the boundary structure showing the positions of most likely segregation of calcium. CaO also exists in the rocksalt structure, meaning that it can easily substitute for magnesium in the boundary plane. Large difference in the ionic sizes of calcium and magnesium means that there is usually little intermixing of CaO and MgO in the bulk. However, in the case of the boundary, the larger ionic size and equilibrium bond length stabilize the structure. Bond–valence analysis predicts a 35% replacement of magnesium with calcium in the boundary plane, consistent with the EELS quantification.

The multiple scattering calculations shown here were performed using commercial FEFF7 codes.[30] These codes use the overlapping-atom prescription of Mattheiss[36] to model the atomic potential within the muffin tin approximation. From the resulting potential, scattering phase shifts and matrix elements are calculated. Core–hole effects are included using the $(Z + 1)^*$ approximation,[31] where * denotes the excited atom. The curves shown are calibrated by alignment of the first spectral feature with experiment, and broadening of 1 eV is added to allow direct comparison with experimental spectra. For the purposes of the calculation, the atomic clusters are divided into shells of atoms where a single shell is composed of atoms that lie between two radii about the excited site. The order of scattering is controlled simply by placing an upper limit on the number of scattering events allowed.

(1) Analysis of Bulk Electronic Structure

Figure 6 shows a comparison of the experimental oxygen *K*-edge with the multiple scattering simulations. The simula-

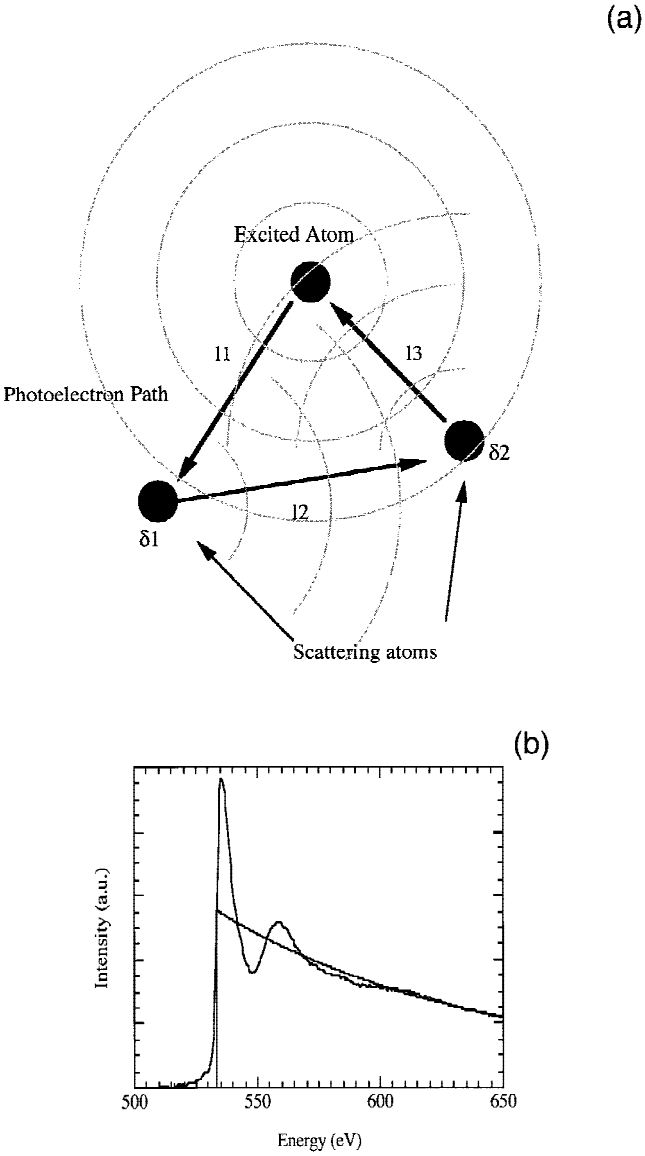

Fig. 5. (a) Multiple scattering calculations model the density of unoccupied states by considering the scattering of the excited photoelectron from neighboring atoms ($L = 11 + \exp(i\delta 1) + 12 + \exp(i\delta 2) + 13$; constructive interference occurs for $L = n\lambda$; destructive interference occurs for $L = (n + 1/2)\lambda$). (b) Resultant energy loss spectrum can be described as a simple absorption edge of hydrogenic form, due to an isolated atom, with intensity modulations due to the atomic structure of the solid.

tions are found to converge after four shells and show very good agreement with the experimental spectrum. To interpret the main features of the oxygen *K*-edge spectrum, we follow the analysis of Rez *et al.*[37] In multiple scattering, the majority of the intensity in the spectrum results from the strongly backscattering oxygen atoms. (Metal atoms are weak scatterers.) The peaks labeled A–C can, therefore, be interpreted as resulting from the following interactions: peak C is the result of single scattering from the nearest-neighbor oxygen atoms, peak B results from single scattering from the fourth shell (second-nearest-neighbor oxygen), and peak A results from multiple scattering from the nearest-neighbor oxygen atoms. This analysis allows a simple interpretation of changes in the fine structure related to coordination and structural disorder. The more

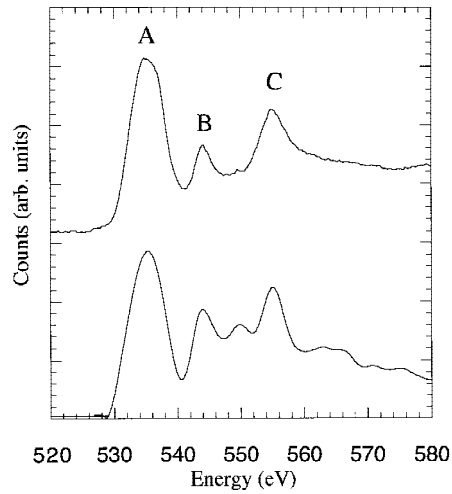

Fig. 6. Comparison of the simulated and experimental bulk oxygen *K*-edge spectra.

disorder in the structure, the greater the effect on second-nearest-neighbor oxygen (i.e., peak B). If the coordination changes, then the biggest effect should be seen in peak A. This is because there are more multiple than single scattering paths that would be eliminated, resulting in peak C. This simple interpretation now permits us to analyze the boundary structure shown in Fig. 4.

(2) Analysis of Boundary Electronic Structure

To analyze the electronic structure of the boundary plane, the clusters used in the multiple scattering analysis must be built up for each atomic column in the boundary. For the structure shown in Fig. 4, the clusters centered on sites 3, 5, 8, 10, 12, and 14 represent all the unique environments in the boundary plane. (The clusters are all centered on the oxygen atoms at these sites.) Fig. 4 shows that, in some cases, these clusters contain a considerable number of calcium atoms as nearest neighbors. In fact, for sites 3 and 5, over half of the nearest neighbors to the central oxygen site are calcium atoms. The multiple scattering simulations from these sites are shown in Fig. 7. Also plotted in Fig. 7 are the multiple scattering simulations for bulk MgO and CaO. In interpreting the multiple scattering spectra from the boundary, we must bear in mind that considerable distortion of the lattice takes place, which can cause the main features of the spectrum to be washed out in some cases. However, it can be seen that the sites with the highest number of calcium atoms in their local environment (3 and 5) show features that are more reminiscent of the bulk CaO structure than of bulk MgO. In a very simple approximation, it appears we can consider these sites as being the location of atomic-scale precipitates of CaO.

The total grain-boundary spectrum can be obtained by summing the spectra from the individual sites. Plotted in Fig. 8 is a comparison of the boundary and bulk multiple scattering simulations. Figure 8 shows that the main feature of the boundary spectrum is a decrease in the intensity of peak A. As we said earlier, a decrease in this peak can be caused by a decrease in the local oxygen coordination. This decrease in coordination for some of the sites in the boundary plane can be most easily seen for the site labeled No. 8 in Fig. 4. (The individual spectrum from this site is shown in Fig. 7.) Here, one of the nearest-neighbor sites (Site 5) is significantly farther away than a comparable site in the bulk. Hence, although the segregation of calcium to specific sites in the grain boundary stabilizes the boundary structure in its present configuration, it cannot completely preserve the bulk coordination for the surrounding boundary sites. However, Fig. 8 shows the effect on the total

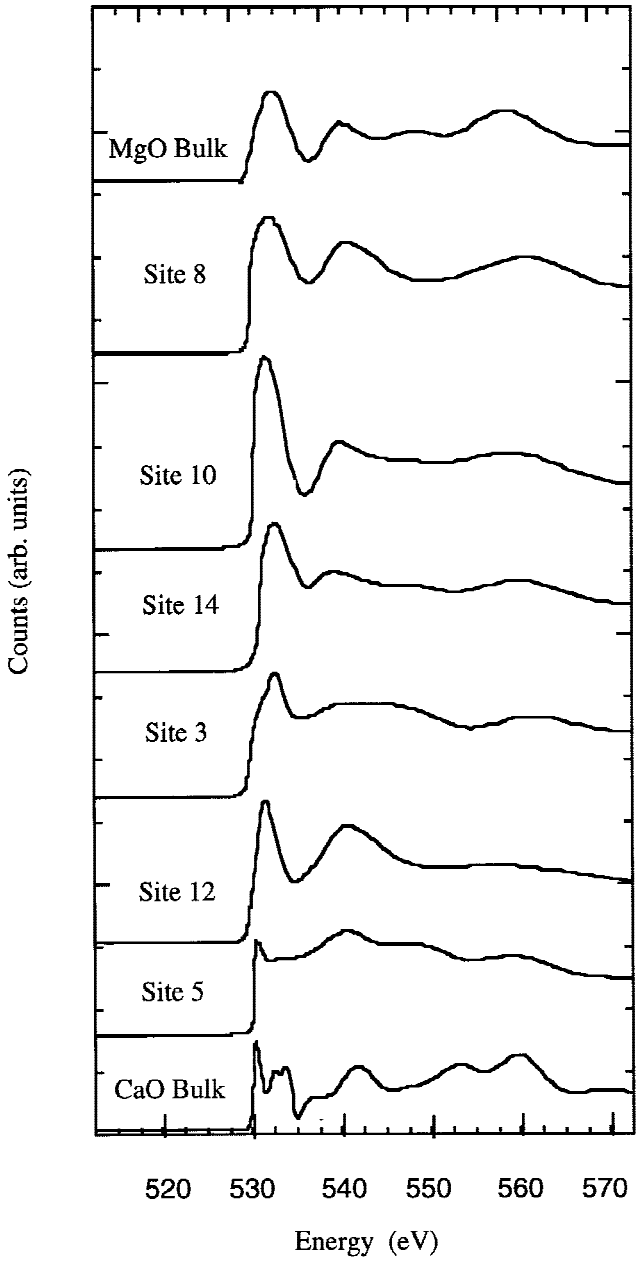

Fig. 7. Simulations of the oxygen *K*-edge for the atomic columns shown in Fig. 4 and Table I. While the majority of the spectra show features consistent with distorted MgO, the sites closest to the segregated calcium show distinct features comparable to the bulk CaO spectrum.

boundary electronic structure is small, and the main features of the bulk oxygen *K*-edge in MgO are maintained.

This analysis begs the question as to why these subtle changes in the oxygen *K*-edge spectrum are not observed in the experimental spectrum. The reason for this most likely lies in the spatial difference technique used to acquire the boundary spectrum. Figure 9 shows the effect of the addition of various levels of bulk oxygen *K*-edge spectrum to the boundary spectrum. When the ratio of bulk to boundary is 4 to 1, the spectrum looks virtually identical to the bulk. In the experimental methodology used here, the ratio of bulk to boundary in the 1 nm × 2 nm area used to acquire the image is well in excess of this ratio. We, therefore, would not expect to be able to observe the changes in the spatial difference technique and must attempt to attain higher spatial resolution. While this is not easy for MgO, because of beam damage, it should be possible for other more stable oxide materials.

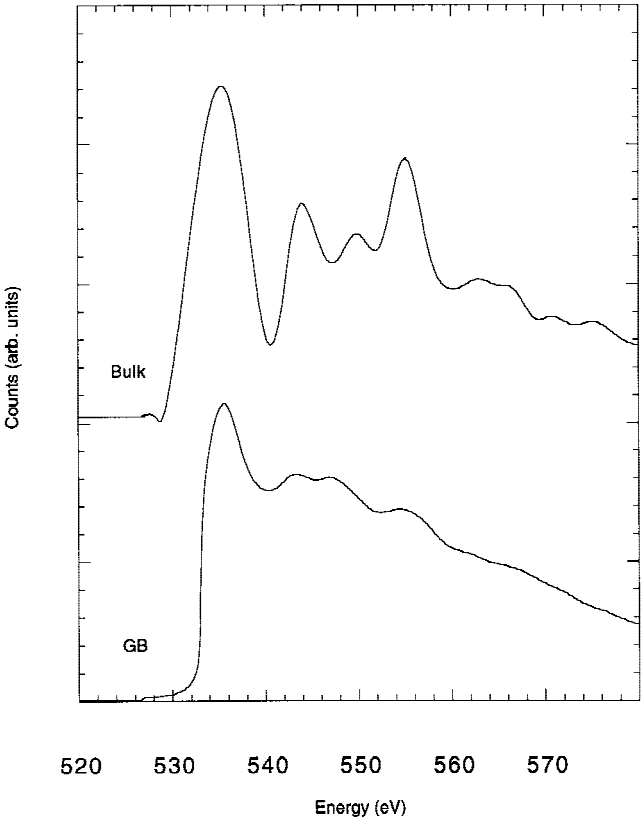

Fig. 8. Comparison of the simulated bulk and boundary spectra.

VI. Discussion and Conclusions

The above analysis suggests that, on a very basic level, we can consider this particular grain-boundary structure in MgO to be stabilized by atomic-scale precipitates of CaO. In the case of CaO and MgO, although they both crystallize in the rocksalt structure individually, the difference in ionic sizes between Mg^{2+} and Ca^{2+} leads to a 14% difference in lattice parameter for the two materials. This large difference means that together they do not form a complete solid solution, with the maximum solid solubility of CaO in MgO at any temperature being of the order of 8%.[4] This high level of immiscibility suggests that CaO is most prevalent at surfaces and grain boundaries, where the high degree of lattice strain allows it to be accommodated. It is also well-known that small precipitates form in a shape that minimizes overall strain energy. To do this effectively at a grain boundary, where strain is nonuniform, the precipitates must have a morphology that is only one or two unit cells wide but runs through the entire thickness of the crystal. This is exactly the behavior that is observed here, where the small regions of CaO relieve the excess strain that would be present if the boundary consisted of only magnesium and oxygen.

Having seen that the boundary consists of CaO precipitates, we can ask what effect this has on conduction in this mixed ionic and electronic conductor.[38] Whether the bulk of the grains are intrinsic or extrinsic, the dominant aspect of the ionic part of total conduction is the migration of magnesium vacancies. Obviously, at the grain boundary some of the potential sites for the hopping of magnesium vacancies are occupied by calcium ions. The excess ionic size of calcium with respect to magnesium suggests that the calcium ions are essentially immobile compared to the magnesium ions. Hence, ionic conduction at the grain boundary is reduced. Furthermore, using this structure as a guide, we can deduce what the effect is of the addition of donor or acceptor ions at the boundary. In the case of donor ions, such as Al^{3+}, there are no sites at the boundary that suggest preferential segregation takes place, and the total

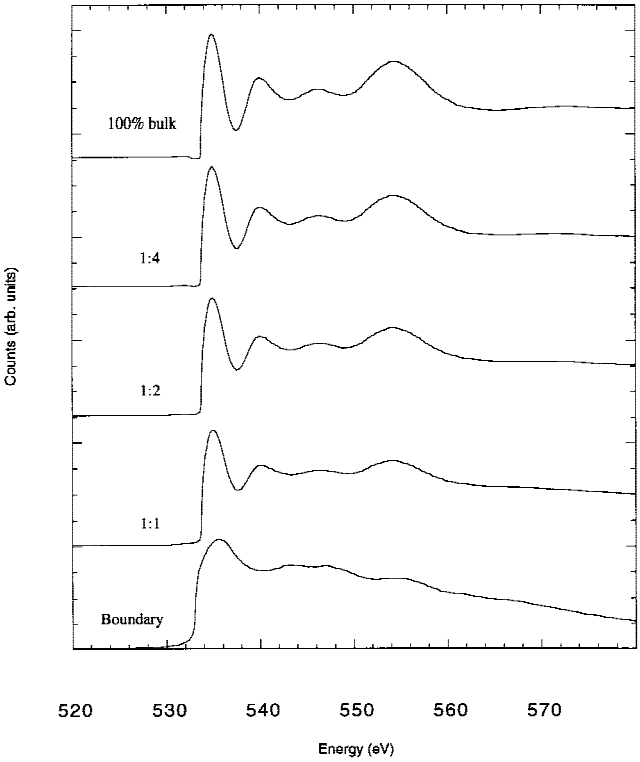

Fig. 9. Comparison of the boundary spectrum with the simulated integrated boundary spectrum with (a) no bulk sites, (b) 1:1 boundary:bulk, (c) 1:2 boundary:bulk, (d) 1:4 boundary:bulk, and (e) 100% bulk.

effect on conduction in this case is limited again to the effect on the migration of magnesium ions. In the case of acceptor ions, such as Na^+, could segregate to the grain boundary. The positions occupied by calcium ions in this structure could just as easily be occupied by the Na^+ ions that are similar in size to the Ca^{2+} ions. In this case, the boundary is electrically active and has a far greater effect on conduction.

In conclusion, we have shown that the bond–valence analysis parameter is analogous to the Born–Mayer potential for small distortions away from the equilibrium bond length. Using this parameter, we can incorporate a wealth of high-resolution experimental information on the atomic structure, composition, and valence state of the cations at grain boundaries into a single comprehensive model. In this study of an MgO [001] tilt boundary, calcium segregants are located at specific locations in the grain-boundary plane, where they could be considered as forming atomic-scale precipitates of CaO. The presence of these precipitates stabilizes the structure of the boundary by minimizing the strain energy of the boundary (because of the longer equilibrium bond length) that would be associated with a pure MgO boundary. This analysis can be equally well applied to other oxide grain boundaries and can be used as the basis to interpret local structure–property relationships.

Acknowledgments: We would like to thank S. J. Pennycook for provision of the experimental facilities necessary to perform the EELS analysis.

References

[1]W. Heywang, ''Resistivity Anomaly in Doped Barium Titanate,'' *J. Am. Ceram. Soc.*, **47**, 484–90 (1964).

[2]See for example, *Ferroelectric Thin Films* II, Material Research Society Symposia Proceedings. Edited by A. I. Kingon, E. R. Myers, and B. Tuttle. Materials Research Society, Pittsburgh, PA, 1991.

[3]J. O. Willis, R. D. Ray II, J. F. Bingert, D. S. Phillips, R. J. Beckman, M. G. Smith, R. J. Sebring, P. A. Smith, B. L. Bingham, J. Y. Coulter, and D. E. Peterson, ''Processing Factors for High Critical Current Density Bi-2223/Ag Tapes,'' *Physica C (Amsterdam)*, **278**, 1–10 (1997).

[4]Y.-M. Chiang, D. Burnie III, and W. D. Kingery, *Physical Ceramics.* Wiley, New York, 1997.

[5]A. P. Sutton and R. W. Balluffi, *Interfaces in Crystalline Materials*. Oxford Press, Oxford, U.K., 1995.

[6]K. L. Merkle and D. J. Smith, ''Atomic Structure of Symmetric Tilt Grain Boundaries in NiO,'' *Phys. Rev. Lett.*, **59**, 2887–90 (1987).

[7]H. Ichinose and Y. Ishida, ''Observation of [110] Tilt Boundary Structures in Gold by High Resolution HVEM,'' *Philos. Mag. A*, **43**, 1253–54 (1981).

[8]K. P. Trumble and M. Rühle, ''The Thermodynamics of Spinel Interphase Formation at Diffusion-Bonded Ni/Al_2O_3 Interfaces,'' *Acta Metall Mater.*, **39**, 1915–24 (1991).

[9]K. J. Morrissey and C. B. Carter, ''Faceted Grain Boundaries in Al_2O_3,'' *J. Am. Ceram. Soc.*, **67**, 292–301 (1984).

[10]D. E. Jesson and S. J. Pennycook, ''Direct Imaging of Interfacial Ordering in Ultrathin $(Si_m,Ge_n)_p$ Superlattices,'' *Phys. Rev. Lett.*, **66**, 750–53 (1991).

[11]N. D. Browning and S. J. Pennycook, ''Direct Experimental Determination of the Atomic Structure at Internal Interfaces,'' *J. Phys. D: Appl. Phys.*, **29**, 1779–98 (1996).

[12]M. M. McGibbon, N. D. Browning, M. F. Chisholm, A. J. McGibbon, S. J. Pennycook, V. Ravikumar, and V. P. Dravid, ''Direct Determination of Grain Boundary Atomic Structure in $SrTiO_3$,'' *Science (Washington, D.C.)*, **266**, 102–104 (1994).

[13]Y.-M. Chiang and T. Takagi, ''Grain-Boundary Chemistry of Barium Titanate and Strontium Titanate: I, High-Temperature Equilibrium Space Charge,'' *J. Am. Ceram. Soc.*, **73**, 3278–85 (1990).

[14]N. D. Browning, M. F. Chisholm, and S. J. Pennycook, ''Atomic-Resolution Chemical Analysis Using a Scanning Transmission Electron Microscope,'' *Nature (London)*, **366**, 143–46 (1993).

[15]V. Ravikumar, R. P. Rodrigues, and V. P. Dravid, ''Space-Charge Distribution across Internal Interfaces in Electroceramics Using Electron Holography: II, Doped Grain Boundaries,'' *J. Am. Ceram. Soc.*, **80**, 1131–38 (1994).

[16]D. M. Duffy and P. W. Tasker, ''Computer Simulation of [001] Tilt Grain Boundaries in Nickel Oxide,'' *Philos. Mag. A*, **47**, 817–25 (1983).

[17]D. J. Harris, G. W. Watson, and S. C. Tarker, ''Atomistic Simulation of the Effect of Temperature and Pressure on the [001] Symmetric Tilt Grain Boundaries of MgO,'' *Philos. Mag. A*, **74**, 407–18 (1996).

[18]L. Pauling, *The Nature of the Chemical Bond*, 3rd ed. Cornell, Ithaca, NY, 1960.

[19]I. D. Brown, ''Chemical and Steric Constraints in Inorganic Solids,'' *Acta Crystallogr., Sect. B: Struct. Sci.*, **48**, 553–72 (1992).

[20]D. Altermatt and I. D. Brown, ''The Automatic Searching for Chemical Bonds in Inorganic Crystal Structures,'' *Acta Crystallogr., Sect. B: Struct. Sci.*, **41**, 240–44 (1985).

[21]I. D. Brown and D. Altermatt, ''Bond–Valence Parameters Obtained from a Systematic Analysis of the Inorganic Crystal Structure Database,'' *Acta Crystallogr., Sect. B: Struct. Sci.*, **41**, 244–47 (1985).

[22]M. Born and J. E. Mayer, ''Zur Gittertheorie der Ionenkristalle,'' *Z. Phys.*, **75**, 1–19 (1932).

[23]Y. Yan, M. F. Chisholm, G. Duscher, and S. J. Pennycook, ''Atomic Structure of a 27° [001] Tilt Grain Boundary in MgO,'' *J. Electron. Microsc.*, in press.

[24]H. Müllejans and J. Bruley, ''Improvements in Detection Sensitivity by Spatial Difference Electron Energy Loss Spectroscopy at Interfaces in Ceramics,'' *Ultramicroscopy*, **53**, 351–60 (1994).

[25]R. F. Egerton, *Electron Energy Loss Spectroscopy in the Electron Microscope*, 2nd ed. Plenum, New York, 1996.

[26]J. K. Burdett and T. Fässler, ''Pair Potentials, Electron-Pair Repulsions, and the Geometries of Molecules,'' *Inorg. Chem.*, **30**, 2859–68 (1990).

[27]V. Heine, I. J. Robertson, M. C. Payne, *Bonding and Structure of Solids.* Edited by R. Haydock, J. E. Inglesfield, and J. B. Pendry. The Royal Society of London, London, U.K., 1991.

[28]C. R. A. Catlow and W. C. Mackrodt (Eds.) *Computer Simulation of Solids.* Springer–Verlag, New York, 1982.

[29]J. K. Burdett, *Chemical Bonding in Solids*. Oxford Press, Oxford, U.K., 1995.

[30]J. J. Rehr, S. I. Zabinsky, and R. C. Albers, ''High-Order Multiple-Scattering Calculations of X-ray-Absorption Fine Structure,'' *Phys. Rev. Lett.*, **69**, 3397–400 (1992).

[31]R. Brydson, H. Sauer, W. Engel, J. M. Thomas, and E. Zeitler, ''Coordination Fingerprints in Electron Energy Loss Near-Edge Structures: Determination of the Local Site Symmetry of Aluminum and Beryllium Ultrafine Minerals,'' *J. Chem. Soc., Chem. Commun.*, **15**, 1010–12 (1989).

[32]R. Brydson, H. Sauer, and W. Engle, ''Electron Energy Loss Near Edge Structure as an Analytical Tool—The Study of Minerals''; pp. 131–54 in *Transmission Electron Energy Loss Spectrometry in Materials Science.* Edited by M. M. Disko, C. C. Ahn, and B. Fultz. TMS, Warrendale, PA, 1992.

[33]H. Kurata and C. Colliex, ''Electron-Energy-Loss Core-Edge Structures in Manganese Oxides,'' *Phys. Rev. B: Condens. Matter*, **48**, 2101–108 (1993).

[34]H. Kurata, E. Lefevre, C. Colliex, and R. Brydson, ''Electron Energy-Loss Near-Edge Structure in the Oxygen *K*-Edge Spectra of Transition-Metal Oxides,'' *Phys. Rev. B: Condens. Matter*, **47**, 13763–68 (1993).

[35]A. Bianconi, ''XANES Spectroscopy for Local Structures in Complex Systems''; pp. 118–29 in *EXAFS and Near Edge Structure.* Edited by A. Bianconi, L. Incoccia, and S. Stipcich. Springer–Verlag, New York, 1983.

[36]L. Mattheiss, ''Energy Bands for Solid Argon,'' *Phys. Rev. [Sect.] A*, **133**, 1399–403 (1964).

[37]P. Rez, X. Weng, and H. Ma, ''The Interpretation of Near Edge Structure,'' *Microsc. Microanal. Microstruct*, **2**, 143–51 (1991).

[38]D. Sempolinski and W. D. Kingery, ''Ionic Conductivity and Magnesium Vacancy Mobility in Magnesium Oxide,'' *J. Am. Ceram. Soc.*, **63**, 664–69 (1980). □